PDAC-on-chip for in vitro modeling of stromal and pancreatic cancer cells crosstalk

PDAC-on-chip for modeling *in vitro* the stromal and pancreatic cancer cells crosstalk

Received 00th January 20xx,
Accepted 00th January 20xx

DOI: 10.1039/x0xx00000x

Viola Sgarminato[a], Simone Marasso[b,c], Matteo Cocuzza[b,c,d], Giorgio Scordo[b,‡], Alberto Ballesio[b], Gianluca Ciardelli[a,d,e], Chiara Tonda-Turo[a,d,*]

Pancreatic ductal adenocarcinoma (PDAC) mainly develops in the head of the pancreas, within the acino-ductal unit composed by acinar and ductal cells surrounded by pancreatic stellate cells (PSCs). PSCs strongly influence the tumor microenvironment by triggering an intense stromal deposition which plays a key role in tumor progression and limits the drugs perfusion. Here, we developed a microfluidic *in vitro* model recreating the *in vivo* tumor-stroma crosstalk to replicate the steps of PDAC evolution towards the establishment of an efficient *in vitro* platform for innovative therapies validation. The multilayer PDAC-on-chip was designed to culture the PDAC cells and the PSCs embedded in a type I collagen gel in the top and bottom layers, respectively. The presence of a biomimetic nanofibrous membrane in the middle of the chip permits to control the interactions between the two cell lines and to easily analyze the effect of the crosstalk on cell behavior. First, the PDAC-stromal cells relationship was evaluated under co-culture conditions on 24-well inserts including the PCL/Gel electrospun membrane. This simplified model shows that the human fibroblasts change their morphology and secrete higher amount of IL-6 cytokines in presence of tumor cells confirming the activation of stromal cells under co-culture. Then, the PDAC-on-chip system was validated by demostrating that human fibroblasts seeded in a 3D collagen matrix in the bottom microchannel also change to a myofibroblasts-like shape with increased expression of α-SMA and secrete higher amount of IL-6 cytokines. Finally, this microfluidic system resulted suitable for the evaluation of drugs efficacy and serves as a powerful tool to understand the early evolution steps of PDAC.

Introduction

Pancreatic ductal adenocarcinoma (PDAC), commonly known as pancreatic cancer, is the most frequent type of exocrine pancreas tumor and one of the leading cause of cancer-related death worldwide with a five-year survival rate of below 9%[1,2].
The main reason that leads to consider PDAC a notably aggressive disease concerns the rapid cancer's evolution without clear symptoms in the early stages, resulting in a late diagnosis and poor clinical prognosis. Indeed, only 10% of the patients has resettable tumors since the majority of cases present extended metastases and advanced lesions at diagnosis[3]. In addition, the genetic complexity and the heterogeneity of the pancreatic tumor microenvironment weaken the effectiveness of the current treatments that, despite the improvements in the discovery of new therapeutical strategies, result insufficient in contrasting this pathology[3–5]. In particular, the PDAC microenvironment is mainly composed by a desmoplastic stroma which strongly affects the tumor's evolution and represents a barrier against chemotherapy and radiotherapy[6–9]. The stroma is mainly composed by collagens, with the type I and III fibrillar collagens accounting for >90% of all collagen mass[10], and it is generated by the excessive extracellular matrix (ECM) deposition principally from the pancreatic stellate cells (PSCs) that trigger an intense desmoplastic reaction within the tissue surrounding the cancer cells[9,11]. More specifically, PSCs are normally located in the periacinar space around the acinar and ductal cells constituting the pancreatic adenomere, which represents the fundamental unit of the exocrine pancreas and the region where the pancreatic intraepithelial neoplasia (PanIN) occurs[3,12]. During the tumorigenesis, the PSCs that are in a quiescent state become active and change their morphology in a spindle-shaped, exhibiting a myofibroblasts-like phenotype. Their primary activation is the result of an inflammatory stimulus which causes the recruitment of the immune system cells into the tumor site (monocytes, T cells, neutrophils, macrophage, and mast cells). The inflammatory cells produce cytokines such as the Interleukin 6 (IL-6), which causes the mutation of the oncogene KRAS and the progression from PanIN to PDAC[6,13]. Although important risk factors can contribute to the evolution of the pancreatic cancer (like smoking, obesity, type 2 diabetes, chronic pancreatitis, and alcoholism[7]) and mechanisms of maturation from the neoplasia are well documented[14,15], the alterations that give rise to the early lesions remain still unclear[16]. For these reasons, current research is focusing on the development of PDAC *in vitro* models for a deeper understanding of this pathology, the identification of new biomarkers and the establishment of screening tests, in order to enable an earlier detection of pancreatic cancer and to improve the prognosis[17–22]. However, one of the major limitations of PDAC *in vitro* models is the lack in replicating the tumor microenvironment surrounding the gland and the PDAC-stroma crosstalk, which constitutes an important feature as it

[a] *Department of Mechanical and Aerospace Engineering, Politecnico di Torino, Turin, Italy*
[b] *Chilab - Materials and Microsystems Laboratory, Department of Applied Science and Technology (DISAT), Politecnico di Torino, Chivasso (TO), Italy*
[c] *CNR-IMEM, Parco Area delle Scienze, Parma, Italy*
[d] *POLITO BIOMedLAB, Politecnico di Torino, Turin, Italy*
[e] *Department for Materials and Devices of the National Research Council, Institute for the Chemical and Physical Processes (CNR-IPCF UOS), Pisa, Italy*
[‡] Present address: *Department of Electrical Engineering and Information Technology, Institute of Sensor and Actuator Systems, TU Wien, Wien, Austria*
**E-mail: chiara.tondaturo@polito.it*
†Electronic Supplementary Information (ESI) available: [details of any supplementary information available should be included here]. See DOI: 10.1039/x0xx00000x

significantly affects the tumor's evolution and the drugs resistance[22–26]. Among the existing *in vitro* models, organ-on-a-chip microfluidic systems represent a powerful tool to reproduce the cancer cells-stroma interactions in a controllable environment and under real-time monitoring[19,27–29]. In addition, these devices make drug tests and cell analysis accessible and immediate due to the presence of typical micrometer-sized channels that allow a controlled patterning of stromal and cancer cells[30]. Recent studies have demonstrated the possibility to include the stromal component on microfluidic platforms to better replicate the PDAC microenvironment by integrating hallmarks of the pancreatic cancer desmoplastic tissue[20,31–34]. However, the research is still far from the complete understanding of this disease and of the mechanisms involved in the PDAC-stroma relationship. Further improvements are therefore needed in the design of microfluidic systems. In this study, a novel biomimetic PDAC-on-chip was designed to model the pancreatic cancer and its interaction with the surrounding environment. In particular, PSCs were embedded in a type I collagen gel and cultured in bottom microchambers of the multilayered device, designed to both confine the gel (the central microchannel) and to guarantee the nutrients transport in automated and dynamic conditions (the two lateral microchannels). The ductal cancer cells, on the other hand, were seeded in the top layer of the platform and they were allowed to grow on a nanofibrous polycaprolactone/gelatin (PCL/Gel) membrane, which represents a biomimetic substrate since the ECM-like architecture typical of the electrospun matrices is able to support cell adhesion, spreading and functions[35–38]. The blend of a synthetic thermoplastic polymer (PCL) and a natural polymer (Gel) has been widely adopted in the fabrication of nanofibrous scaffolds as it allows to achieve a combination of suitable mechanical and physicochemical properties with an improved biocompatibility[39–42]. Moreover, the presence of the electrospun membrane in the middle of the chip permits to control the interactions between the two cell lines and to easily analyze the effect of the crosstalk on cell behavior. This aspect was also evaluated by implementing the co-culture conditions on 24-well inserts before proceeding with the experiments in the microfluidic system. In particular, preliminary assays were performed on commercial inserts modified by replacing the polyethylene terephthalate (PET) membrane with the PCL/Gel nanofibrous mat and used to investigate the activity of human fibroblasts and human ductal cells (wild type or KRAS-mutated) seeded in mono- or co-culture.

Experimental Section

Cell culture

Human pancreatic ductal epithelial cells (HPDE) stably expressing activated KRAS (HPDE-KRAS) and wild-type HPDE (HPDE-wt) were kindly provided by Prof. F. Bussolino and cultured in RPMI-1640 medium (Gibco, Thermo Fisher Scientific, Waltham, USA) supplemented with 1% Penicillin-Streptomycin (Gibco), 1% L-glutamine (Gibco) and 10% fetal bovine serum (FBS) (Gibco). Human foreskin fibroblasts (HFF1) cells were obtained from ATCC® and cultured in Dulbecco's Modified Eagle's Medium (DMEM) supplemented with 1% Penicillin-Streptomycin (Gibco), 2% L-glutamine (Gibco) and 15% FBS (Gibco). PSCs were purchased from iXCells Biotechnologies (San Diego, USA) and cultured in Stellate Cell Growth Medium kit (iXCells Biotechnologies, San Diego, USA) composed by Stellate Cell Basal Medium supplemented with 0.2% Stellate Cell Growth Supplement, 1% Penicillin-Streptomycin-Amphotericin B Solution 100x and 10% FBS. Cell lines were maintained in a humidified CO_2 incubator at 37 °C and 5% CO_2.

Preparation of modified transwell inserts using the PCL/Gel electrospun membrane

Electrospun membrane. The PCL/Gel membrane was produced via solution electrospinning, in accordance with previously optimized protocols[35]. In brief, PCL/Gel solution at 15% w/v was prepared mixing the PCL and Gel polymers (respectively in the ratio of 80:20 w/w) in a mixture of acetic acid and formic acid in the ratio of 1:1 v/v. GPTMS (3-glycidoxypropyltrimethoxysilane) was added as gelatin crosslinker to the final solution in a concentration of 3.68% v/v[38,43]. The electrospinning process was performed by employing the NovaSpider instrument (CIC nanoGUNE, San Sebastian, Spain) and the parameters were set, in accordance with earlier tests, at 12 kV voltage, 0.5 ml/h flow rate and 12 cm distance.

PCL/Gel nanofibers were integrated on the commercial 24-well inserts. Specifically, each insert was modified by removing the polyethylene terephthalate (PET) membrane and leaving only the polystyrene support. The electrospun membranes were then cut in small square pieces and applied on the plastic inserts by employing poly-dimethylsiloxane (PDMS; Sylgard 184, Dow Chemical, Midland, USA) to favor the adhesion. In order to avoid an excessive impregnation of membranes with PDMS, a thin layer of PDMS was brushed on the insert's outer walls and a first pre-crosslinking was performed by maintaining the supports at 90 °C for about 5 min. After the positioning of the PCL/Gel fibers on the polystyrene supports, an additional layer of PDMS was applied on the edges of the membranes and they were then kept at 70 °C for about 2 min to complete the curing of PDMS.

Cell seeding in transwell inserts

The transwell inserts modified with PCL/Gel electrospun membranes were sterilized *via* UV light for 1h before cell seeding. Cells were cultured both on the PCL/Gel electrospun membrane modified supports (TW_PCL/Gel) and on the commercial 24-well PET inserts (TW_PET) with 8.0 μm pore size, 0.1×10^6 per cm^2 pore density and 0.3 cm^2 growth area. HFF1, HPDE-WT and HPDE-KRAS were seeded in mono- and co-culture. The co-culture medium was prepared in accordance with preliminary tests performed to individuate the appropriate concentration of supplements (Fig. S1). In particular, they were maintained in DMEM/F-12 supplemented with 15% FBS (Gibco), 1% Penicillin-Streptomycin (Gibco) and 2% L-glutamine (Gibco). The 1:3 ratio of HPDE-WT and HPDE-KRAS to HFF1 cells was adopted for the co-culture conditions. The human fibroblasts and the ductal cells were seeded at densities of 3×10^4 cells/transwell and 1×10^4 cells/transwell, respectively. In

particular, 35 µL of medium containing HFF1 and 20 µL of medium containing HPDE-KRAS or HPDE-wt were respectively pipetted on the upper and lower side of the membrane. After seeding the cells were allowed to adhere for approximately 1h at 37 ° C and 5% CO_2 before adding the medium both in the inner and the outer compartments of the modified inserts. The medium was refreshed every 2 days during the culture.

Interleukin 6 (IL-6) cytokines release

Cytokines' concentration was determined in cell supernatants that were collected from the upper side of the TW_PET and TW_PCL/Gel membranes after 24h, 48h, 72h and 7d of culture using the IL-6 Human ELISA Kit (Thermo Fisher Scientific, BMS213-2). The concentrations were calculated using the standard curve generated by plotting the absorbance values of each standard sample on the ordinate and the human IL-6 standard concentrations on the abscissa. This assay has allowed to quantify the IL-6 cytokines released by cells seeded both on TW_PET and TW_PCL/Gel in mono- and co-culture.

Morphological analysis of HFF1 seeded on TW_PET inserts

Fluorescence imaging was carried out to analyze the changes in cell morphology of human fibroblasts seeded in co-culture with HPDE-KRAS on the commercial PET transwell inserts (TW_PET). The inserts were washed once with 1x phosphate-buffered saline (PBS; Gibco) and fixed with 4% paraformaldehyde (PFA) (Sigma Aldrich) for 30 min at room temperature, after 24h, 48h and 72h of culture. They were then washed twice with 1x PBS, permeabilized in 0.5% Triton X-100 (Sigma Aldrich) in 1x PBS for 10 min and incubated with 1% bovine serum albumin (BSA; Thermo Fisher Scientific) for 30 min to improve the staining. The cytoskeletons of HPDE-KRAS and HFF1 were stained with Alexa Fluor™ 488 Phalloidin (Thermo Fisher Scientific, A12379) at 1:60 concentration in 1x PBS with 1% BSA solution while nuclei were visualized with DAPI reagent (4',6-Diamidino-2-Phenylindole, Dihydrochloride; Thermo Fisher Scientific, D1306) at 1:1000 concentration in 1x PBS solution. All samples were then imaged by confocal microscopy (Eclipse Ti2, Nikon). The aspect ratios of HFF1 cells both in mono- and co-culture were also measured using Fiji (version 1.53c).

Embedding stromal cells into the collagen gel

Collagen gel solution (10 mg/ mL) was prepared by mixing sterile collagen type I from bovine hides (FibriCol®, Advanced Biomatrix, Carlsbad, USA) with 10x phosphate-buffered saline (PBS; Gibco) and sterile distilled water. The pH was adjusted to 7.4 using 0.1 M NaOH. Cells were embedded into the collagen gel at densities of 1 x 10^6 cells/ml (D1), 3 x 10^6 cells/ml (D2) and 5 x 10^6 cells/ml (D3). To compare the viability of human fibroblasts seeded at D1, D2 and D3 inside the collagen gel, the CellTiter-Glo® 3D Cell Viability Assay (Promega, Milano, Italy) was performed according to the manufacturers' protocols. In addition, the LIVE/DEAD™ Assay (Thermo Fisher Scientific) was carried out on the cells loaded within the collagen gel at the density which resulted optimal, in order to further confirm the quantitative test (metabolic activity assay) results. Images were acquired with a fluorescent cell imager (ZOE™; Bio-Rad, Hercules, USA) and analyzed using Fiji (version 1.53c). The HFF1 cells were harvested and embedded in the type I collagen solution at a final density of 3 × 10^6 cells/ml. The same procedure was adopted to embed the PSCs in the collagen gel.

Design and fabrication on the multilayer microfluidic device

The microfluidic device, composed by a bottom layer and a top layer connected by an electrospun membrane, was firstly designed by Rhinoceros® (Robert McNeel & Associates) CAD software and then fabricated by replica molding. Briefly, poly-dimethylsiloxane (PDMS; Sylgard 184, Dow Chemical, Midland, USA) base and crosslinking agent were mixed thoroughly at a ratio of 10:1 w/w and poured onto the master mold and cured for 3h at 60 °C. An additional layer was successively introduced to allocate the medium reservoirs, whose mold was fabricated through a laser cutter (Microla slider) on a polymethylmethacrylate (PMMA) substrate.

Bottom Layer. The mold of the bottom layer was obtained by SU-8 photolithography. Briefly, an SU-8 patterned master was custom-made using photolithography and then conventional soft lithography was applied to produce several PDMS replicas. The bottom layer has three channels: a central compartment (6.38 mm length, 1 mm width and 250 µm height) delimited by micropillars, with 100 µm diameter and 250 µm height and two lateral channels (20.51 mm length, 500 µm width and 250 µm height).

Top Layer. The top layer was obtained by laser machining in a laser cutter (Microla slider) on a 3 mm thick PMMA substrate.

Electrospun membrane. The PCL/Gel membrane was produced via solution electrospinning, as previously described.

The chip has been assembled through a plasma oxygen treatment of the PDMS surfaces to decrease the hydrophobicity and therefore facilitate the bond between the different layers. The electrospun PCL/Gel membrane was inserted between the top and bottom layers to create an ECM-like substrate for epithelial cell growth.

Fluidic characterization of the bottom layer

Liquid insertion and diffusivity tests were performed to evaluate the influence of the distance between the pillars on the retention of the gel within the middle microchannel and the diffusivity of the medium from the lateral to the central channels, respectively. In particular, gaps of 50 µm and 75 µm between the pillars were analyzed.

Insertion test. A solution of deionized water and blue food dye was loaded into the inlet of the central channel in the bottom layer through a manual micropipette and under an optical microscope (Leica M205 A, Leica Microsystems, Wetzlar, Germany) to monitor confinement of the liquid inside the microchannel. This test was repeated by loading the colored acellularized collagen gel within the middle channel.

Diffusivity test. The acellularized collagen gel was loaded into the central channel while a fluorescent solution was prepared by adding a blue emitting dye to deionized water. Successively, 10

µL of fluorescent solution was inserted in the lateral channels and the chip was observed with an inverted confocal microscope (Eclipse Ti2, Nikon, Amsterdam, Netherland). Images were acquired every 30 seconds for 30 minutes and the fluorescence intensities at different time points were calculated as mean value of pixels measured in six regions of interest (ROIs), that cover 60% of the effective area in the central channel.

Cell seeding in the microfluidic device

The platform was treated with UV light for 1h as sterilization process before cell culture.

Stromal cells. PSCs were loaded into the central channel of the bottom layer by injecting 3 µL of cell-hydrogel mixture at a density of 10×10^3 cells/channel. After polymerization at 37 °C and 5% CO_2 for about 40 min, the lateral microchannels in the bottom layer and the reservoirs were filled with culture medium and returned to the incubator for culture. Sterile PBS was added into the wells to avoid dehydration of the hydrogel. Medium was changed every day.

Ductal cells. HPDE-KRAS cells were seeded in the top layer on the PCL/Gel electrospun membrane at a density of 35×10^3 cells/channel by pipetting 5 µL of medium with cells inside the chamber. The chips were then placed in incubator for about 30 min to enhance attachment of cells to the nanofibers. Successively, the reservoirs were filled with culture medium and returned to the incubator. Medium was changed every day during the culture period.

Co-culture. Stromal cells (HFF1 and PSCs respectively) and cancer ductal cells (HPDE-KRAS) were co-cultured in the assembled multilayer chip. A 1:3 ratio of cancer cells to stromal cells was used since it has been reported as a commonly adopted value due to the relevancy that ratios of 1:1 to 1:3 have *in vivo* [44–46]. Particularly, densities of 3.5×10^3 cells/channel and 10×10^3 cells/channel were used for cancer and stromal cells respectively. Cells were co-cultured and maintained in DMEM/F-12 supplemented with 15% FBS (Gibco), 1% Penicillin-Streptomycin (Gibco) and 2% L-glutamine (Gibco) since previous tests demonstrated the efficacy of this culture medium composition in promoting the cell viability (Fig. S1). Stromal cells were embedded in the type I collagen gel as previously described and loaded in the central chamber of the bottom layer by using the inlet on the top layer corresponding to the central channel in the bottom layer. HPDE-KRAS cells were seeded by injecting 5 µL of medium with cells inside the inlet corresponding to the chamber in the top layer. Reservoirs were filled with culture medium and medium was changed every day during the culture period.

Viability of cells inside the platform was analyzed by LIVE/DEAD assay at different time points. In particular, cells seeded within the microfluidic platforms and on the common polystyrene multiwell cell culture plate (controls) were incubated with LIVE/DEAD™ reagents (Thermo Fisher Scientific) according to the manufacturer's protocol. The PSCs embedded in the type I collagen gel and seeded in a plastic multiwell plate were also stained and used as control. Subsequently, the cultures were imaged by employing ZOE™ fluorescent cell imager. Fluorescence staining and imaging were also performed to evaluate the morphology and the spatial distribution of HPDE-KRAS and PSCs seeded in the microfluidic platforms, both in mono- and co-culture, at different time steps. Each compartment of the device was washed once with 1x PBS (Gibco) and fixed with 4% PFA (Sigma Aldrich) for 30 min at room temperature. After washing twice with 1x PBS, the chambers were filled with 0.5% solution of Triton X-100 (Sigma Aldrich) in 1x PBS and maintained for 10 min at room temperature to allow cell membrane permeabilization. Then, samples were incubated with 1% BSA (Thermo Fisher Scientific) for 30 min to improve the staining. The cytoskeletons of cells in monoculture were visualized using the green-fluorescent Alexa FluorTM 488 Phalloidin (Thermo Fisher Scientific, A12379) while the actin filaments of cells seeded in co-culture were stained with Rhodamine Phalloidin (Thermo Fisher Scientific, R415) at 1:60 and 1:400 concentrations in solutions of 1x PBS with 1% BSA, respectively. Nuclei were observed with DAPI reagent (Thermo Fisher Scientific, D1306) as previously described. Images were acquired by confocal microscopy (Eclipse Ti2, Nikon) and analyzed using Fiji (version 1.53c).

Administration of tumor supernatant to human fibroblasts seeded in the bottom layer

HFF1 embedded in type I collagen gel and seeded in the bottom layer of the microfluidic device were treated with supernatant collected from TW_PCL/Gel seeded with HPDE-KRAS in monoculture after 72h. Indeed, the tumor supernatant was administered to HFF1 after 48h of culture in the bottom layer. The same procedure was applied to HFF1 embedded in the type I collagen gel and seeded in a plastic multiwell plate, as control. The expression of alpha smooth muscle actin (α-SMA) was determined by immunofluorescence staining. Briefly, cultures in microchannels and in the controls were fixed after 48h of incubation with HPDE-KRAS supernatant using 4% PFA for 30 min and further treated with 0.5% Triton X-100 for 10 min. After blocking non-specific binding with 1% BSA, the primary antibody against α-SMA (1:100, Sigma Aldrich, A7607) was applied for overnight incubation at 4 °C. After incubation with Goat anti-Mouse IgG1 Secondary Antibody (1:1000, Thermo Fisher Scientific, SA5-10264), Alexa FluorTM 488 Phalloidin (Thermo Fisher Scientific, A12379) and DAPI (1:1000, Thermo Fisher Scientific, D1306), samples were analyzed by confocal microscopy (Eclipse Ti2, Nikon). The images were then analyzed and the fluorescence intensity (mean gray values) distribution was plotted using the Fiji software. In addition, the concentration of IL-6 cytokines released by HFF1 seeded in the bottom layer of the microfluidic chip was quantified using the IL-6 Human ELISA Kit (Thermo Fisher Scientific, BMS213-2) after 48h of incubation with the HPDE-KRAS supernatant.

Testing the drug efficacy to induce HPDE-KRAS cell death using PDAC-on-chip

HPDE-KRAS were cultured in the top layer as previously described. To test the effect of anti-cancer agents on the cell

viability, 100 nM bortezomib (SelleckChem, Houston, USA) and 1 µM gemcitabine (SelleckChem, Houston, USA) in the HPDE growth medium were injected in the inlet corresponding to the microchamber of the top layer. HPDE-KRAS grown for 48h were treated with drug for 24h and 96h and they were successively stained using LIVE/DEAD™ reagents (Thermo Fisher Scientific) in accordance with the manufacturer's instructions.

Statistical Analysis

All bar graph data are presented as the mean ± standard deviation (SD) for at least two independent experiments (n ≥ 2) with at least three replicates per time point. Significance was measured as indicated for each experiment, with two-way or one-way ANOVA followed by pairwise comparison with Tukey's multiple comparisons test using GraphPad Prism 9.3.1; *p < 0.05, **p < 0.01, ***p < 0.001, ****p < 0.0001.

Results

Increased IL-6 cytokines release by human fibroblasts under co-culture conditions

In order to evaluate the effect of the interaction between the human fibroblasts and the ductal cells, the concentration of IL-6 cytokines was measured through the ELISA test (Fig. 1) by

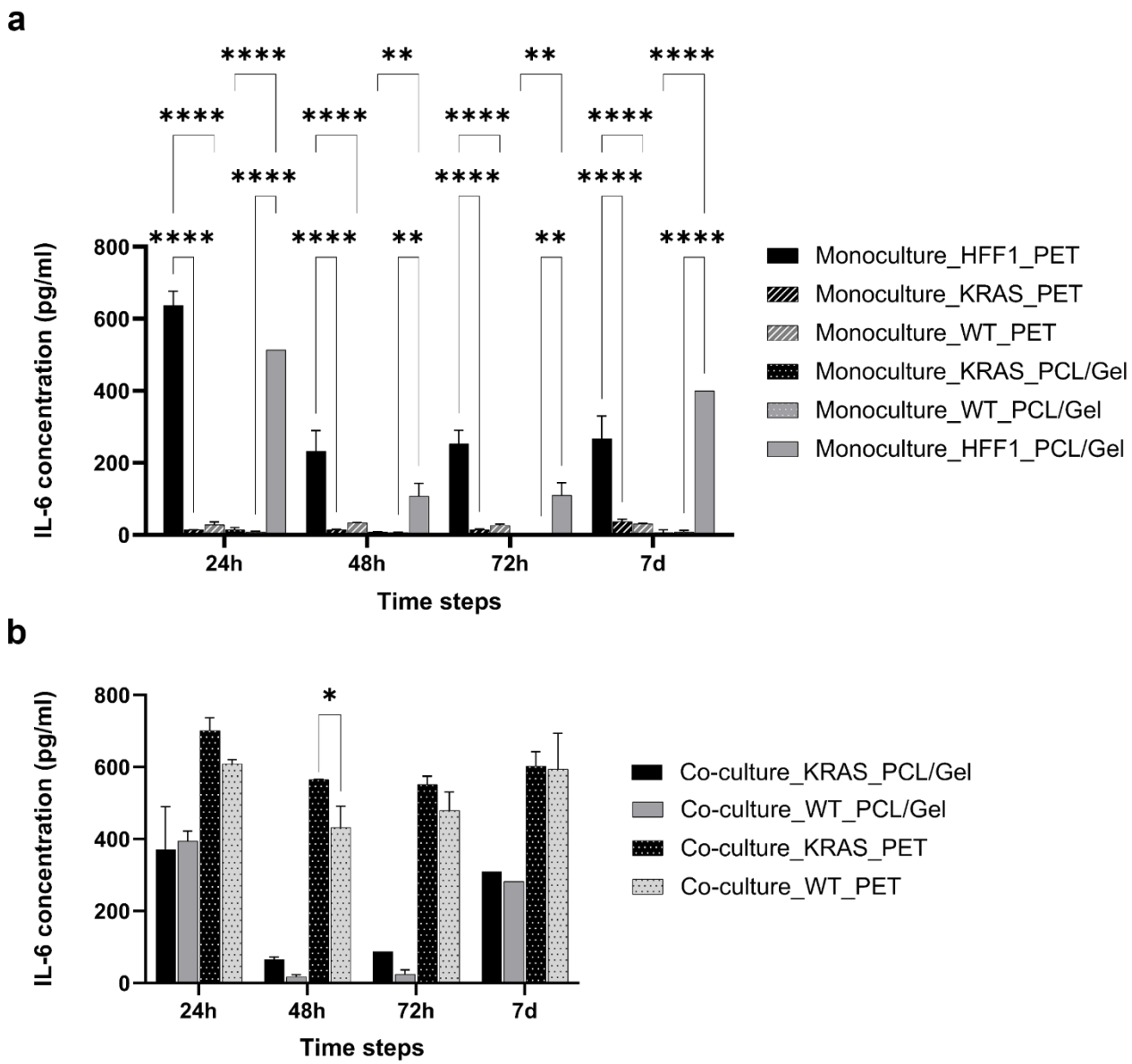

Fig. 1 IL-6 cytokines concentration in supernatants collected from mono and co-culture in the transwell inserts. Bar plots of the data obtained from ELISA test IL-6 analysis for each culture condition on TW_PET (a) and TW_PCL/Gel (b) grouped per time step (n=2). Tukey's multiple comparisons test: *p < 0.05, **p < 0.01, ***p < 0.001, ****p < 0.0001.

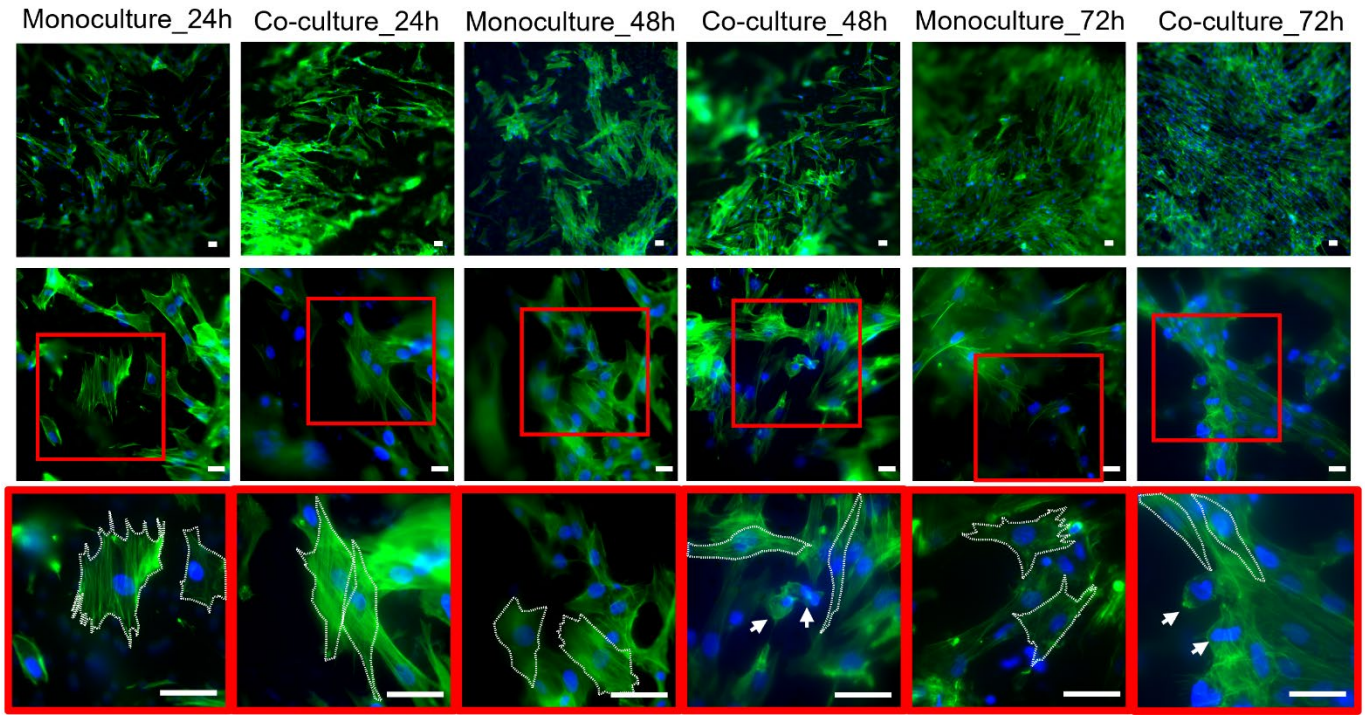

Fig. 2 Effect of tumor-stroma crosstalk on human fibroblasts morphology. Representative confocal images at different magnifications (20X, 60X and 100X) obtained upon the HFF1 and HPDE-KRAS staining of nuclei (DAPI) and F-actin (Alexa Fluor™ 488 Phalloidin) in monocultures (HFF1) and co-cultures (HFF1+HPDE-KRAS) after 24h, 48h and 72h from seeding. The white arrows in the images at 100X indicate the HPDE-KRAS cells in co-culture with the human fibroblasts. Scale bars 50 µm.

analyzing the supernatants of HFF1, HPDE-KRAS and HPDE-wt seeded in mono and co-culture on TW_PCL/Gel and TW_PET inserts. The highest amount of IL-6 released by cells under monoculture (Fig. 1a) have been quantified at 24h after seeding on the TW_PET membranes by HFF1 cells. After 24h, 48h and 72h from seeding, the IL-6 concentration analyzed in the monoculture HFF1 medium on the TW_PCL/Gel membranes resulted significantly lower compared to the TW_PET. This behavior could be ascribed to the more biomimetic architecture (Fig. S2) and composition of electrospun nanofibers compared to PET, which reduces the fibroblast activation after cell culturing. The amount of IL-6 determined in the media of HPDE-KRAS and HPDE-wt in monoculture resulted minimal (Fig. 1a) for all the tested conditions. In general, the most consistent release of cytokines has been quantified in the supernatant of HFF1 in co-culture with the HPDE-KRAS cells (Fig. 1b). The same trend has been observed on the TW_PCL/Gel membranes, although the concentrations are lower than those measured on the TW_PET membranes.

Morphological changes of human fibroblasts co-cultured with HPDE cells on the transwell inserts

Confocal imaging at different magnifications was performed to analyze the effect of tumor-stroma crosstalk on fibroblasts morphology (Fig. 2). As expected, HFF1 seeded on the TW_PET inserts have showed changes in cytoskeletal organization when cultured with the HPDE-KRAS cells. Indeed, the human fibroblasts assumed a more spindle-shaped conformation from 24h to 72h after seeding and in comparison with the monocultures, as confirmed by the aspect ratio measurements (Fig. S3).

Viability of stromal cells embedded in type I collagen gel

CellTiterGlo 3D Assay and LIVE/DEAD Assay were performed to evaluate the viability of fibroblasts loaded within the type I collagen gel and cultured for one week (Fig. 3). Fig. 3a shows that cells seeded at a density of 3 x 10^6 cells/ml (D2) resulted more viable and active compared to those seeded at a lower density of 1 x 10^6 cells /ml (D1). In addition, the D2 density resulted better than a higher density D3 (5 x 10^6 cells/ml) as the cell viability increased with time resulting in optimal fibroblasts survival and proliferation within the gel. LIVE/DEAD images were acquired at 3 x 10^6 cells/ml (Fig. 3b-d) showing an increment in cell number during the culture period, confirming the optimal proliferative capability of fibroblasts embedded in the collagen gel at a density of 3 x 10^6 cells/ml (Fig. 3b-d). In particular, accordingly with the viability assay (Fig. 3a), cells were able to grow throughout the culture period, creating fibrillar and compact structures within the tridimensional (3D) framework (Fig. 3d).

Development of a functional multilayer device

The fabrication of the PDMS microfluidic system was carried out as previously illustrated. The platform consists of a top and a

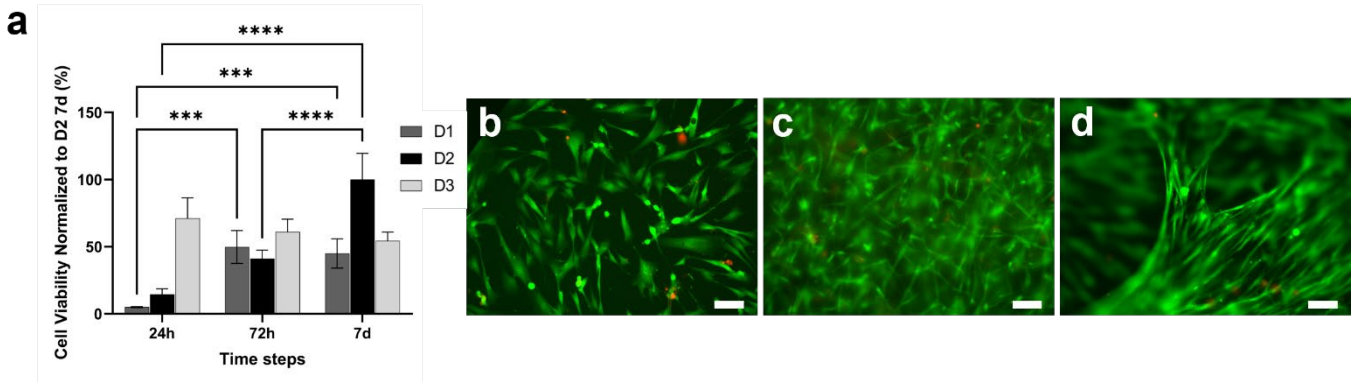

Fig. 3 Human fibroblasts viability in type I collagen gel. (a) Comparison between the viability of HFF1 seeded at D1 (1 x 10^6 cells/ml), D2 (3 x 10^6 cells/ml) and D3 (5 x 10^6 cells/ml) densities (n=3). Tukey's multiple comparisons test: ***p < 0.001, ****p < 0.0001. (b-d) LIVE/DEAD images of HFF1 (3 x 10^6 cells/ml) embedded in the gel at 24h (b), 72h (c) and 7d (d) after seeding. Cells were stained using calcein-AM for live cells and ethidium homodimer-1 for dead cells. Images are representative of at least six individual regions of the gels (n=3). Scale bars 100 µm.

bottom layer divided by an electrospun PCL/Gel membrane (Fig. 4).

Top Layer. The final dimensions of the microchannel resulted 12 mm length, 400 µm width and 500 µm height. Inlets and outlet allocated at this level have 2.2 mm diameters (Fig. 4).

Bottom Layer. The bottom layer has three channels: a central compartment (6.38 mm length, 1 mm width and 250 µm height) delimited by micropillars, with 100 µm diameter and 250 µm height, that aim to confine a collagen gel loaded with the PSCs and two lateral channels (20.51 mm length, 500 µm width and 250 µm height) to control the nutrients passage (Fig. 4b). The Field Emission Scanning Electron Microscopy (FESEM) images (Fig. 4b, i-iii) allowed to evaluate the repeatability of the SU8-photolithograhy process which has permitted to achieve high resolutions in terms of micropillars dimensions and geometrical accuracy. In addition, digital microscopy confirmed the support given by the two rows of pillars in maintaining the PCL/Gel membrane flat in the assembled chip configuration (Fig. 4c). The bottom layer was also characterized to determine the influence of the distance between the pillars on the retention of the gel within the middle microchannel and the diffusivity of the medium from the lateral to the central channels. As reported in Fig. 5, both water-based liquids and collagen hydrogel resulted confined into the central microchamber, for the two pillars gaps tested (50 µm and 75 µm). On the other hand, the diffusivity test allowed to establish the optimal distance between the micropillars, by analyzing the diffusion of a fluorescent solution from the lateral channels to the middle chamber containing the type I collagen gel (Fig. 5b-f). Fig. 5b-c show the measurements of the fluorescence intensity at different time intervals for the two layouts (50 µm and 75 µm pillars gaps). The average fluorescence intensity of the analyzed ROIs was indicated as I0 at time t0= 0s, while for t > 0s it was generically indicated as I. The first peaks of intensity are due to the initial addition of the fluorescent dye. The trend is linear for both layouts, indicating a uniform diffusion within the collagen gel for both 75 µm and 50 µm inter-micropillars distances. In addition, the angular coefficient of the interpolation line describing the diffusivity coefficient in the collagen gel is the same for both layouts. However, the model with a gap of 75 µm between pillars (Fig. 5b) has proved to be the most promising model as the diffusion is faster and the central channel is completely fluorescent in less than 30 minutes, thus suggesting a good compromise for the nutrients transport to the cells embedded in the gel.

Cell culture in the microfluidic device

The response of PSCs and HPDE-KRAS cells, seeded in the bottom and in the top layers respectively, was evaluated in terms of cell viability, proliferative capability and cell morphology. Precisely, the PSCs embedded in the type I collagen gel and seeded in the central microchannel of the bottom layer (Fig. 6a) were able to colonize the chamber by modelling the hydrogel and forming a dense tissue throughout the duration of the experiment. The LIVE/DEAD images (Fig. 6b) reveal that the stromal cells remained viable and active despite a few dead cells in the initial phase of seeding. This is probably related to the embedding procedure which could be aggressive to the cells, causing a high number of dead cells which is remarkable from 24h to 48h and greatly decrease from 48h to 72h, after seeding. The morphological analyses have demonstrated a uniform spatial distribution of PSCs that exhibit a high degree of cell spreading, developing interconnected multicellular networks (Fig. 6c). Furthermore, the fluorescence images show the migratory ability of stromal cells which cross over the central channel after 4 days from seeding. The ductal

cells stably expressing activated KRAS (HPDE-KRAS) were

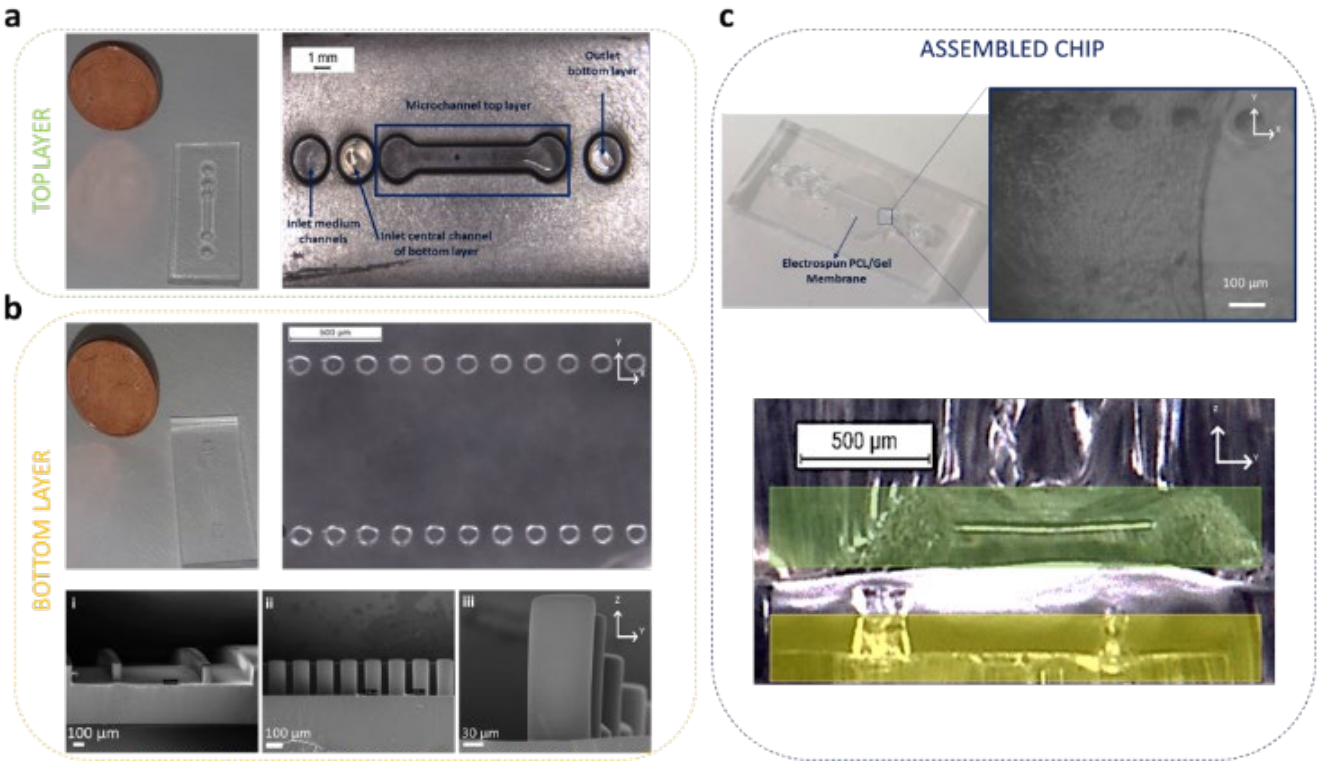

Fig. 4 PDAC-on-chip: multilayer microfluidic device. (a) Top layer with the inlets, the outlet and the microchannel. (b) Bottom layer with the central microchannel delimited by two rows of micropillars (i,ii,iii) and two lateral microchannels. (c) Assembled chip configuration showing the electrospun PCL/Gel membrane inside the device. In the cross view the nanofibrous matrix can be observed between the top layer (green) and the bottom layer (yellow).

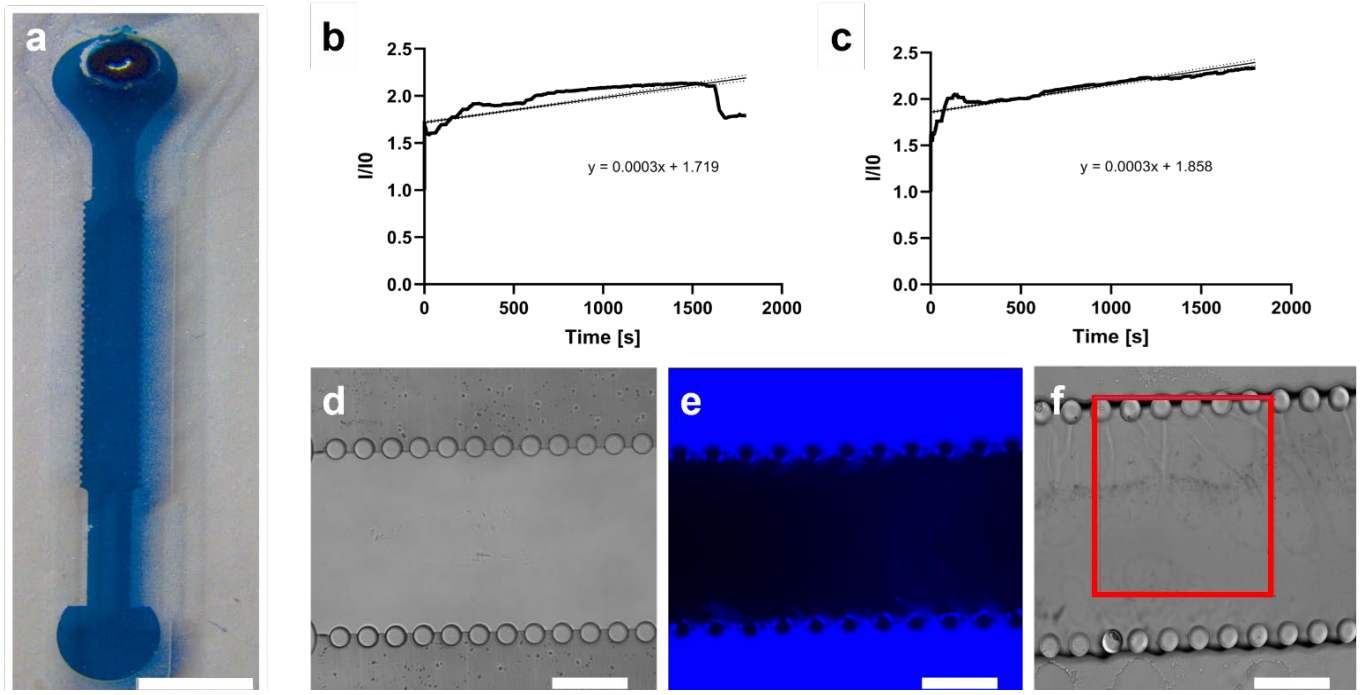

Fig. 5 Fluidic characterization of the bottom layer. (a) Insertion test. Monitoring of the blue colored solution confinement inside the central microchannel. Scale bar 2 mm. (b-f) Diffusivity test. The fluorescence intensity of a stained solution was measured at different time intervals, for two pillars gaps, 75 µm (b) and 50 µm (c). The central chamber was filled with type I collagen gel (d) and the fluorescent solution was injected in the lateral microchannels (E) at t0 = 0 s. The average intensity was calculated considering the values registered in different ROIs (f). Scale bars 200 µm.

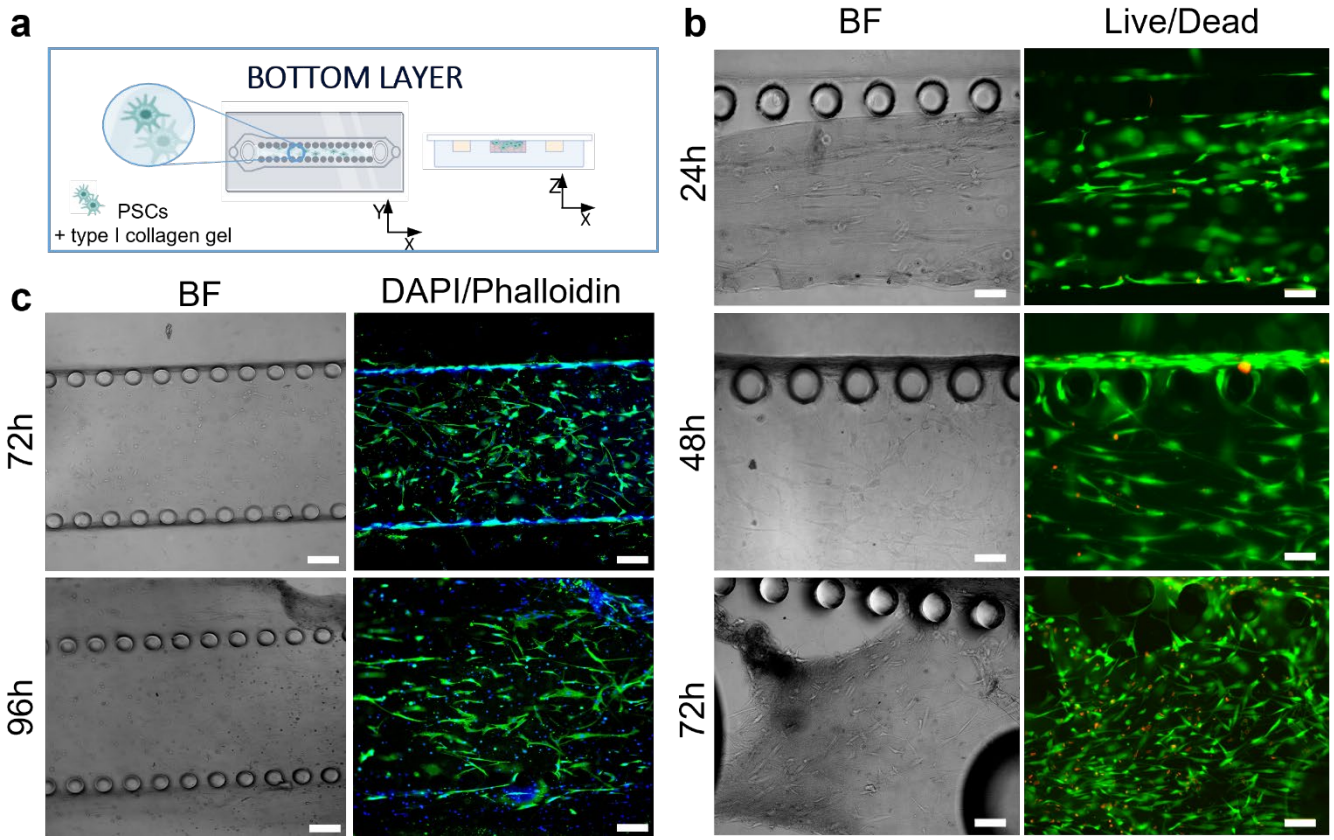

Fig. 6 Seeding of human pancreatic stellate cells (PSCs) within the type I collagen gel in the bottom layer. (a) Schematic illustration of the bottom layer with the central microchannel containing the PSCs embedded in the collagen gel. (b) LIVE/DEAD images showing the viability of stromal cells at 24h, 48h and 72h after seeding (n=3). (c) Representative confocal images of PSCs in brightfield and upon staining with DAPI (nuclei) and Alexa Fluor™ 488 Phalloidin (cytoskeletons) at 72h and 96h after seeding. Scale bars 100 µm.

seeded in the top layer of the microfluidic device (Fig. 7a) to firstly evaluate their biological response in monoculture conditions. In particular, the PCL/Gel electrospun membrane and the overhead PDMS layer were bonded to a glass coverslip in order to better monitor the cell behavior. The LIVE/DEAD assay revealed a good cell viability on PCL/gelatin nanofibers thus confirming the cytocompatibility of membrane which represents an optimal culture substrate for
cell adhesion and proliferation (Fig. 7b). In addition, the cytoskeletal organization of the ductal cells was evaluated by fluorescence microscopy which allowed to observe the formation of the characteristic cobblestone morphology proving that cells were functionally active[47,48] (Fig. 7c). The co-culture condition was implemented in the assembled chip, where the different layers were joined together through a plasma oxygen treatment of the PDMS surfaces (Fig. 8a). Fig.8b shows fluorescence images at higher magnifications where HPDE-KRAS and stellate cells can be observed. In particular, the HPDE-KRAS cells, with their typical cuboidal shape, are well distinguishable as the focal plane observed is the one where they were seeded on the top of the PCL/Gel membrane, while the PSCs (white arrows) result migrated and, in contact with the tumoral cells, display an elongated spindle shape suggesting their possible activation. However, the PSCs are hardly visible and the quality of images reported in Fig. 8b is considerably inferior to those of monocultures. Indeed, the hydrogel tend to impregnate the nanofibrous membrane causing autofluorescence and noising effects in confocal images limiting the detection of cell distribution.

Activation of human fibroblasts cultured with HPDE-KRAS supernatant

The capability of exploiting the chip setup to monitor morphological changes of cells seeded in the bottom layer was demonstrated. HFF1 cells embedded into the collagen gel were biochemically stimulated using supernatant collected from TW_PCL/Gel seeded with HPDE-KRAS in monoculture (Fig. 9). Cell morphology was evaluated and compared with data collected from the TW configurations previously analyzed. As shown in Fig. 9 and Fig. S3, HFF1 assumed an elongated spindle shape indicating their activation when cultured with the HPDE-KRAS supernatant for 48h and upon staining of F-actin. The change in cell morphology can be observed in Fig. 9a and Fig. 9b reporting the cytoskeletons of HFF1 in the microchamber of the bottom layers, cultured with (Fig. 9a) and without (Fig. 9b) the HPDE-KRAS supernatant. This evidence was further confirmed by the increment in α-SMA expression in fibroblasts embedded within the collagen gel and seeded both in the bottom layer and in the

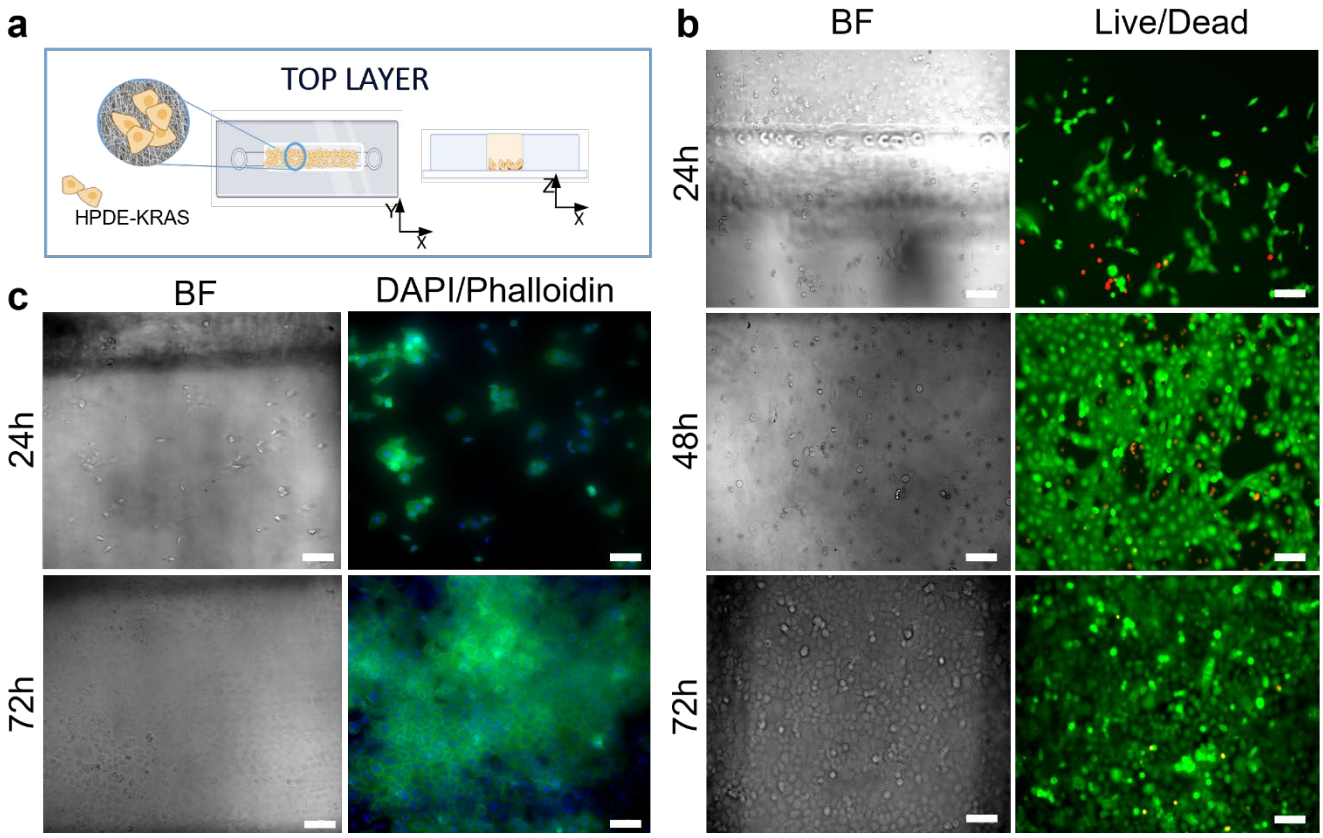

Fig. 7 Seeding of PDAC cells in the top layer. (a) Schematic illustration of the top layer with the HPDE-KRAS cells seeded in the microchannel on the electrospun membrane. (b) LIVE/DEAD images showing the viability of HPDE-KRAS on the nanofibrous matrix in the chip at 24h, 48h and 72h after seeding (n=3). (c) Representative confocal images of HPDE-KRAS grown on the electrospun membrane inside the device upon staining with DAPI (nuclei) and Alexa Fluor™ 488 Phalloidin (cytoskeletons) at 24h and 72h after seeding. Scale bars 100 µm.

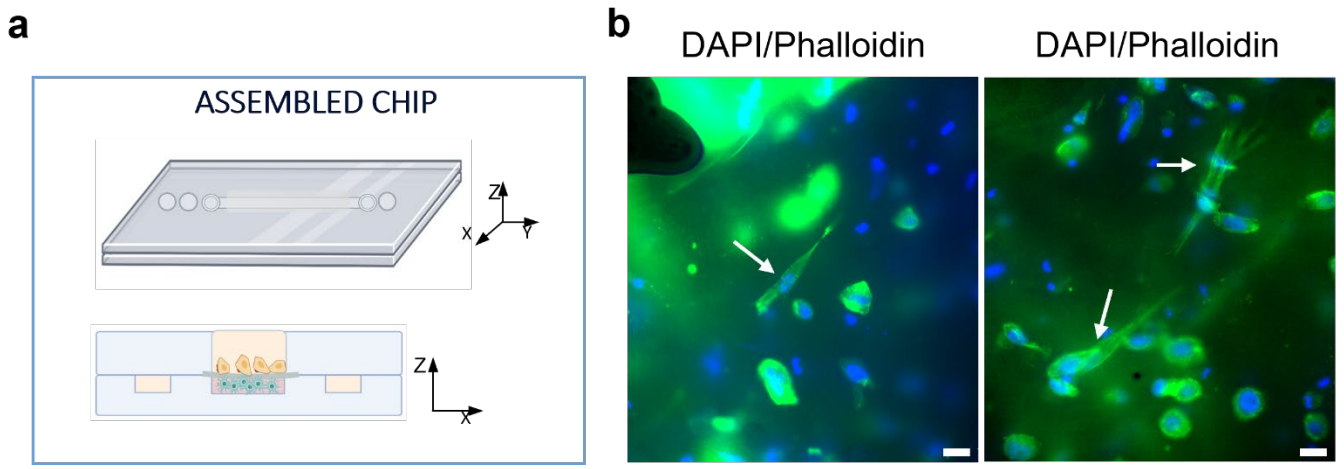

Fig. 8 Seeding of PSCs and HPDE-KRAS in the assembled chip under co-culture conditions. (a) Schematic illustration of the assembled chip with the HPDE-KRAS cells seeded in the top and the PSCs in the bottom layers, respectively. (b) Representative confocal images at high magnifications showing the HPDE-KRAS cells together with the PSCs with elongated spindle shapes, indicated by the white arrows. Scale bars 20 µm.

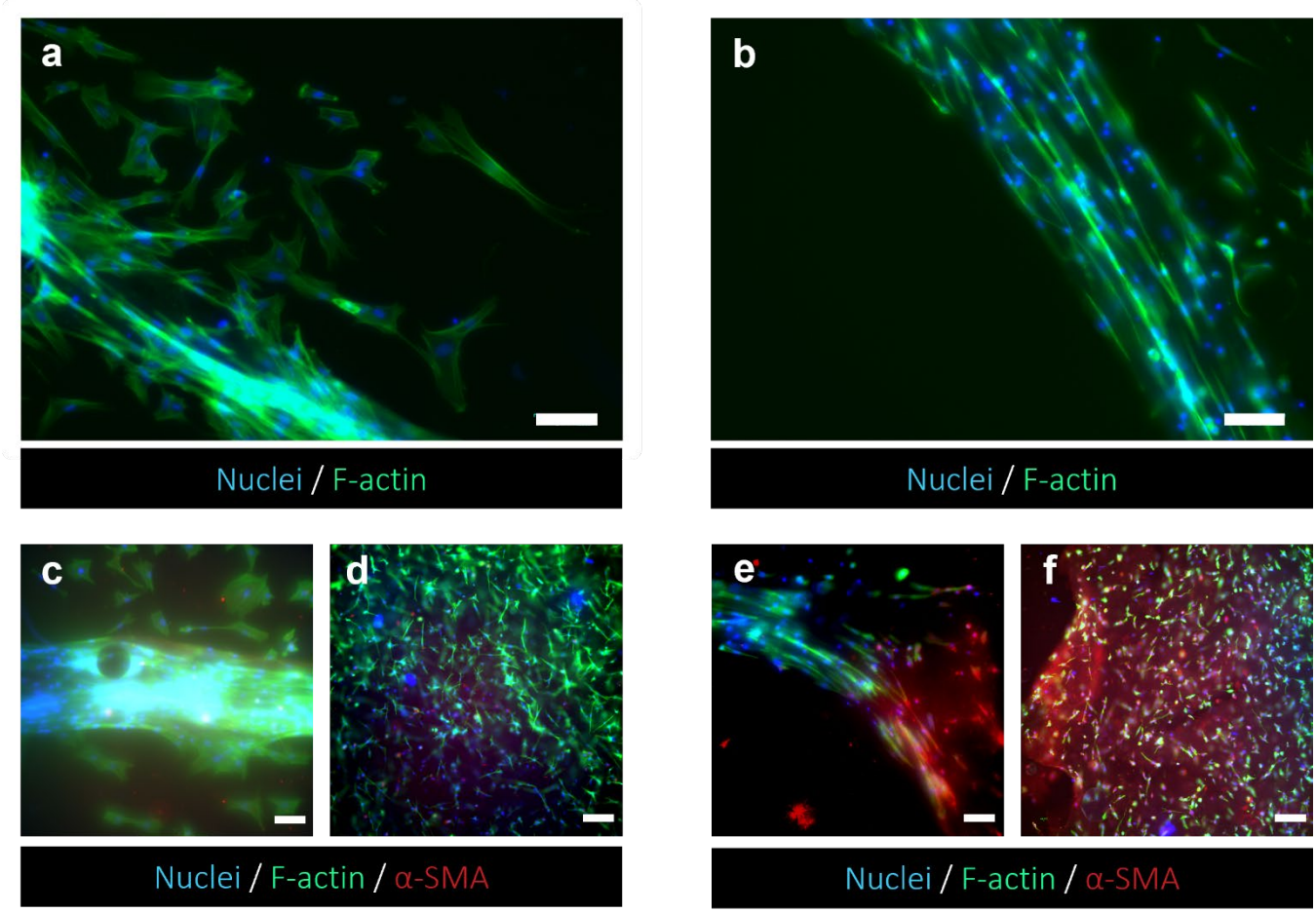

Fig. 9 Activation of human fibroblasts upon culture with HPDE-KRAS supernatant. (a-b) Fluorescent images of HFF1 seeded in the bottom layer of PDAC-on-chip and stained with Alexa Fluor™ 488 Phalloidin (F-actin) and DAPI (nuclei) to highlight the differences between the fibroblasts before (a) and after (b) the incubation with tumor supernatant. Cells were grown for 48h before the staining. Images are representative of at least three individual regions of the same chip. Scale bars 100 µm. (c-f) Representative confocal images showing the changes in morphology and α-SMA expression of HFF1 before (c-d) and after (e-f) the treatment with HPDE-KRAS supernatant. (c,e) HFF1 embedded in collagen hydrogel and seeded in the bottom layer of the microfluidic device. Scale bars 50 µm. (d,f) HFF1 grown within the type I collagen gel in the 24-wells and used as controls. Scale bars 100 µm.

24-wells used as controls (Fig. 9d, f). Indeed, the α -SMA amount is considerably higher in samples incubated with the tumor-derived supernatant (Fig. 9e-f), compared to the "untreated" samples (Fig. 9c-d) confirming the activation of fibroblasts towards a myofibroblast phenotype. In addition, the graphs plotting the grey value measured on fluorescence images show a more homogeneous distribution of the intensity values for the untreated conditions (Fig. S5$a_{i\text{-}iii}$, $b_{i\text{-}iii}$) in comparison to the distributions of the treated samples (Fig. S5$a_{iv\text{-}vi}$, $b_{iv\text{-}vi}$). The peaks visible in Fig. S5a_{vi} and Fig. S5b_{vi} correlate with an evident difference in the fluorescence intensity emitted by cells and background respectively, indicating a higher expression of α-SMA. Moreover, a higher level of IL-6 cytokines was measured in the medium of HFF1 seeded in PDAC-on-chip after the incubation with the pancreatic cancer cells supernatant. Indeed, a25% increment in IL-6 cytokines amount was detected through ELISA kit when HFF1 were treated with HPDE-KRAS supernatants compared to HPDE ones (Fig. S5c).

Drug sensitivity of HPDE-KRAS cultured in the microfluidic device

The HPDE-KRAS response to anti-cancer chemotherapeutic agents was analyzed and the validity of the PDAC-on-chip device in evaluating the drugs efficacy was demonstrated. Indeed, the LIVE/DEAD images (Fig. 10) showed significant changes in viability of cells exposed to bortezomib (Fig. 10a) and gemcitabine (Fig. 10b) after a treatment period of 24h and 96h. The evident decrease in cell number after the drugs treatment was due to cell detachment following the cell apoptosis of pancreatic cancer cells induced by the chemotherapeutic treatment.

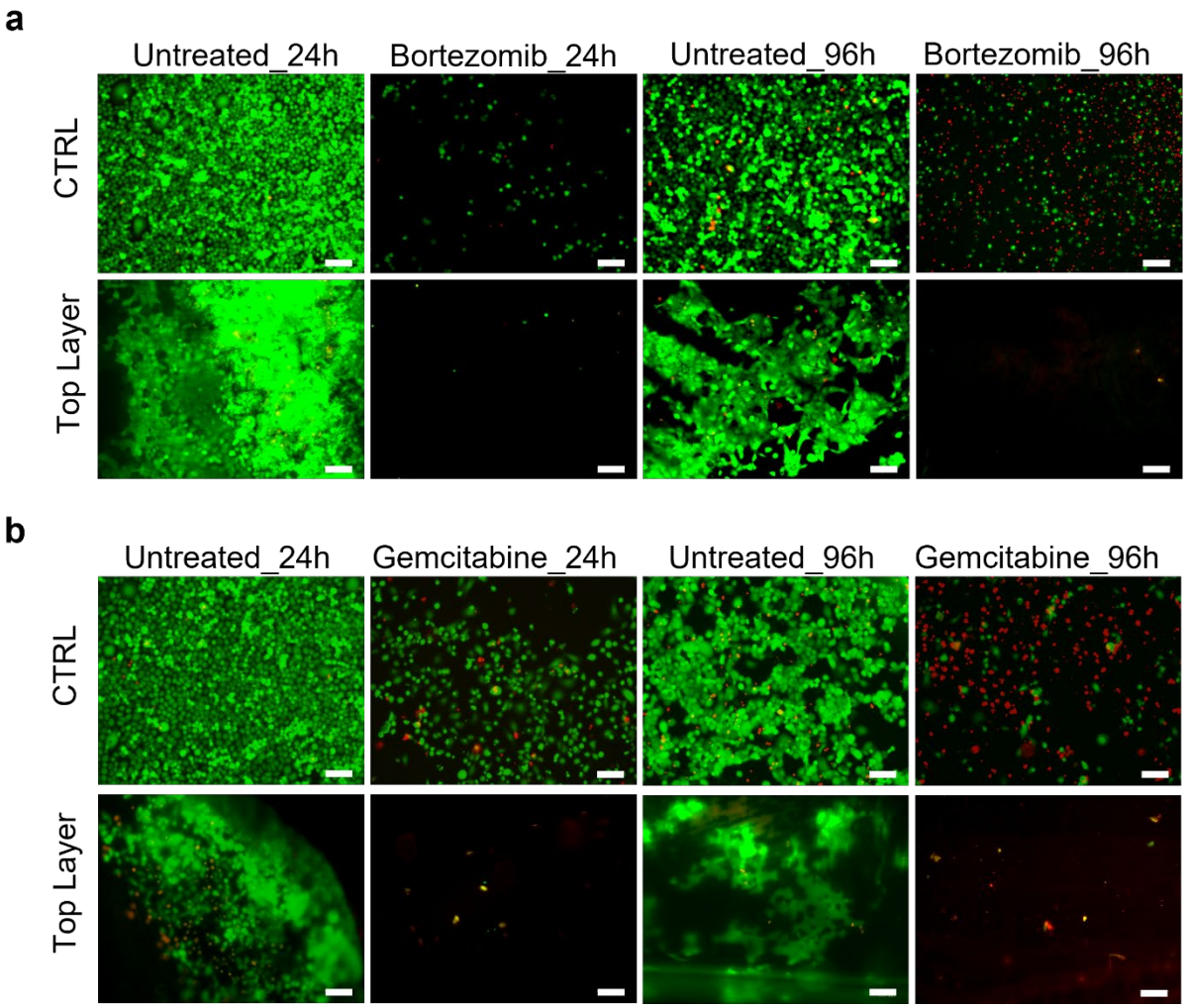

Fig. 10 Sensitivity of HPDE-KRAS cells to anti-cancer drugs. (a-b) Cell viability analyses of HPDE-KRAS grown for 48h and stained with calcein-AM (live cells) and ethidium homodimer-1 (dead cells) after 24h and 96h exposure to gemcitabine (a) and bortezonib (b). Images are representative of at least three individual regions of the same chip. Scale bars 100 µm.

Discussion

The interaction between the pancreatic cancer and the surrounding microenvironment represents a key aspect which has to be investigated to enhance the knowledge of this malignant pathology and improve the efficacy of drug screening[49]. Indeed, as several evidences have demonstrated[50–55], the stroma represents a histopathological hallmark of pancreatic ductal adenocarcinoma and plays a fundamental role in tumor progression[56,57]. Although recent studies have shown the possibility of modeling the PDAC microenvironment *in vitro*[17,20,28,33,34,58–61], the tumor-stroma crosstalk remains extremely challenging to be reproduced and monitored in functionally effective models[62–64].

We report here the design, development and characterization of a multilayer PDAC-on-chip device to mimic the tumor-stroma relationship through the culture of human pancreatic ductal epithelial cells expressing the activated KRAS and human pancreatic stellate cells, on the same miniaturized platform. In particular, the HPDE-KRAS cells and the PSCs were respectively seeded in the top and in the bottom layers, separated by an electrospun PCL/Gel membrane. The effects of the PDAC-stroma crosstalk on cellular behavior were firstly analyzed in terms of fibroblasts activation, that typically occurs during the inflammatory response characterizing the tumor development[65–68]. HFF1 cell line was used to perform these preliminary tests since the differences with the PSCs are minimal[69], with the advantage of major resistance and stability of functions over extended *in vitro* passages. Indeed, despite the genetic differences between the pancreatic stellate cells and the skin fibroblasts[70], the use of fibroblasts from non-pancreatic origins has been helpful for understanding the crosstalk between stromal and cancer cells, as many studies have demonstrated[34,71–74]. The results proved the influence of the co-culture conditions on fibroblasts behavior, corresponding to an increment of IL-6 cytokines release (Fig. 1) and a change in cytoskeletal morphology (Fig. 2). In particular, we quantified a higher IL-6 concentration in the supernatant of HFF1 in co-culture with the HPDE-KRAS cells compared to the

co-culture with healthy ductal cells (HPDE-wt). These outcomes are in line with the data reported by other studies in literature showing that the expression of the oncogenic KRAS correlates with the signaling pathways involved in the inflammatory cascade and in the activation of stromal cells in pancreatic cancer[6,75–77]. Moreover, the IL-6 cytokines play an important role in pancreatic tumor progression and are produced in abundance by components of stroma including PSCs and fibroblasts[6,11,78]. As shown in Fig. 1, an increment of IL-6 produced by HFF1 in co-culture with HPDE-KRAS is noticed, with a significant increase at 48h. These data were also confirmed by the morphological analyses performed on the HFF1 seeded in mono- and co-culture with the HPDE-KRAS on the TW_PET inserts and stained after 24h, 48h and 72h (Fig. 2). Indeed, the human fibroblasts exhibit a more spindle-shaped conformation at 72h in co-culture.

To replicate the composition of the adenocarcinoma microenvironment, the stromal cells were embedded in a type I collagen gel which represents the main constituent of the PDAC stroma[79]. We tested the viability of HFF1 loaded within the gel and we demonstrated that the type I collagen hydrogel exhibits good biological properties in terms of cells viability and growth (Fig. 3), supporting other studies showing enhanced adhesion and proliferation of human fibroblasts embedded within the 3D collagen gels[80,81]. We also observed the capability of stromal cells in remodeling the gel resulting in the formation of tridimensional and compact cellularized hydrogel structures (Fig. 3d).

The collagen gel was then used to incorporate the PSCs seeded within the here designed multilayer microfluidic device (Fig. 4). In particular, the bottom layer was fabricated to insert the hydrogel within the central microchamber, which is delimited by two rows of micropillars (100 µm diameter and 250 µm height) aiming at both gel confinement and nutrients passage (Fig. 4b). The use of a collagen matrix to encapsulate the PSCs seeded in dedicated microchannels was also illustrated in the experimental work of Lee and collaborators[33]. However, in our pancreatic cancer chip model we employed, for the first time, a biomimetic nanofibrous membrane to control the HPDE-KRAS cells interaction with PSCs (Fig. 4c).

In addition, we investigated the fluidic properties of the bottom layer and found 75 µm as the optimal distance between the micropillars, although larger gaps are used in literature [20,44]. Indeed, we have shown that a liquid medium is able to completely diffuse from the lateral microchannel into the central chamber in 30 minutes, thus ensuring the transport of nutrients to the cells in a short time (Fig. 5).

The microfluidic device designed in this work guarantees a good cell survival and it allows to easily monitored the cell response within the chip, key features for a clinically-relevant experimental in vitro model of healthy and pathological tissues. Indeed, the response of PSCs and HPDE-KRAS cells seeded inside the chip was analysed in terms of cell viability, proliferative capability and cell morphology. In particular, the PSCs resulted able to colonize the chamber by growing throughout the duration of the experiment (Fig. 6). However, the tests revealed few dead cells in the initial phase of seeding which could be associated with the embedding procedure in the gel. Thus, the thermal shock given by the temperature of the collagen solution (4 °C) could be the cause of the cell apoptosis occurring during the first hours after seeding[82]. Nonetheless, the stellate cells seem to recover from the stress and continue to proliferate, showing a high degree of cell spreading inside the collagen network (Fig. 6b-c). The confocal microscopy analysis allowed to observe the PSCs flat morphology indicating their viability[83] and the typical stellate shape suggesting their quiescent state in monoculture[6,84]. Focusing on the cell behavior of HPDE-KRAS seeded in the top layer (Fig. 7), we assessed that the PDAC cells remain viable and active as confirmed by the confocal images showing the typical acinar organization of the ductal cells *in vivo*[85] (Fig. 7c). These results underline the importance of a biomimetic substrate like the electrospun PCL/Gel nanofibrous matrix in promoting the epithelial cell viability and functionality, as widely discussed in literature[86–90]. The co-culture conditions implemented in our model have allowed to preliminary evaluate the reciprocal influence that the HPDE-KRAS cells and the PSCs have on each other. Specifically, we observed from the confocal images an increment in PDAC cells migration and the morphological change of stellate cells that appear in a spindle shape indicating their activation, as highlighted in the study of Lee and coworkers[33].

This aspect has been further analyzed by culturing the HFF1 embedded in the type I collagen gel with the HPDE-KRAS supernatant, to correlate the fibroblasts behavior in the PDAC-on-chip device with the one observed on transwell inserts. We found that HFF1 in a 3D collagen matrix change from a relatively short and flat shape to a myofibroblasts-like shape with stress fiber formation and increased expression of α-SMA (Fig. 9). In addition, a higher level of IL-6 cytokines released by HFF1 seeded in PDAC-on-chip was measured. This result contributes to validate the microfluidic system since the fibroblasts cultured inside the bottom layer experience the same stimuli as compared to the HFF1 seeded on TW inserts.

The drug sensitivity of HPDE-KRAS cells cultured in the microfluidic platform was characterized through the exposure to different chemotherapeutic agents. Precisely, we used bortezomib and gemcitabine that are proteosome and DNA synthesis inhibitors respectively[91]. We preliminary assessed the validity of the PDAC-on-chip system which can be used to test the efficacy of drugs on pancreatic cancer cells. Our chip allows the administration of single or multiple drugs both in contact to epithelial, as well as stellate cells, and a continuous monitoring of the effect of the therapeutic treatment on both cell populations can be easily performed thanks to the presence of the electrospun membrane which confined cells in a specific chip compartment.

Finally, in the current tumor-stroma interplay on-a-chip scenario[74], the device developed in this work accurately recapitulates the key aspects of the relationship between the tumor and its microenvironment through a scalable and high-throughput approach. Moreover, the use of a nanofibrous and biomimetic membrane to compartmentalize the microfluidic device and thus separate the cancer component from the stromal tissue allow to study the effect of the inflammation stimuli on the stromal cells in a controlled and specific way.

Conclusions

A multilayer PDAC-on-chip was here designed and developed to model *in vitro* the tumor-stroma crosstalk. Pancreatic stellate cells (PSCs) embedded in a 3D type I collagen matrix and ductal cells expressing the oncogene KRAS (HPDE-KRAS) seeded on a biomimetic nanofibrous membrane, were co-cultured inside the microchannels of the device. The relationship between stromal and ductal cells was evaluated both in the nanofibrous membrane alone and in the chip. Increased level of cytokines, changes in morphology and higher expression of α-SMA were observed when human fibroblasts were cultured with HPDE-KRAS cells or HPDE-KRAS supernatant. Our work thus underlines the biological relevancy that the PDAC-stroma interactions have in determining the tumor microenvironment remodeling during the pancreatic cancer insurgence.

In conclusion, this study provides an *in vitro* model which allows to better study the tumor-stroma reciprocal influence and to perform drug screening towards the identification of effective personalized and high-throughput therapeutical strategies for individual patients. Furthermore, the developed device will allow to carry out additional studies to evaluate the influence of stromal cells seeded in the microfluidic device on drug diffusion.

Author Contributions

VS: Data curation, Formal Analysis, Writing – original draft, Investigation. SM: Conceptualization, Investigation, Funding acquisition, Writing – review & editing. MC: Conceptualization, Investigation, Funding acquisition, Writing – review & editing. GS: Investigation. AB: Investigation. GC: Funding acquisition, Writing – review & editing. CTT: Conceptualization, Formal Analysis, Writing – original draft, Investigation, Methodology, Funding acquisition.

Conflicts of interest

There are no conflicts to declare

Acknowledgements

We thank Prof. V. Cauda and Prof. F. Bussolino for their support in cell culturing. This work was partially performed thanks to the financial support of Deflect project (Piedmont Region).

References

1. Khomiak, A. *et al.* Recent Discoveries of Diagnostic, Prognostic and Predictive Biomarkers for Pancreatic Cancer. *Cancers (Basel).* **12**, 3234 (2020).
2. Siegel, R. L., Miller, K. D. & Jemal, A. Cancer statistics, 2020. *CA. Cancer J. Clin.* **70**, 7–30 (2020).
3. Orth, M. *et al.* Pancreatic ductal adenocarcinoma: Biological hallmarks, current status, and future perspectives of combined modality treatment approaches. *Radiation Oncology* vol. 14 1–20 (2019).
4. Brunet, L. R., Hagemann, T., Andrew, G., Mudan, S. & Marabelle, A. Have lessons from past failures brought us closer to the success of immunotherapy in metastatic pancreatic cancer? *Oncoimmunology* **5**, (2016).
5. Heinrich, M. A., Mostafa, A. M. R. H., Morton, J. P., Hawinkels, L. J. A. C. & Prakash, J. Translating complexity and heterogeneity of pancreatic tumor: 3D in vitro to in vivo models. *Adv. Drug Deliv. Rev.* **174**, 265–293 (2021).
6. Apte, M. V., Wilson, J. S., Lugea, A. & Pandol, S. J. A starring role for stellate cells in the pancreatic cancer microenvironment. *Gastroenterology* **144**, 1210–1219 (2013).
7. Nielsen, M. F. B., Mortensen, M. B. & Detlefsen, S. Key players in pancreatic cancer-stroma interaction: Cancer-associated fibroblasts, endothelial and inflammatory cells. *World Journal of Gastroenterology* vol. 22 2678–2700 (2016).
8. Watt, J. & Kocher, H. M. The desmoplastic stroma of pancreatic cancer is a barrier to immune cell infiltration. *Oncoimmunology* **2**, (2013).
9. Weniger, M., Honselmann, K. C. & Liss, A. S. The extracellular matrix and pancreatic cancer: A complex relationship. *Cancers* vol. 10 (2018).
10. Liot, S. *et al.* Stroma Involvement in Pancreatic Ductal Adenocarcinoma: An Overview Focusing on Extracellular Matrix Proteins. *Frontiers in Immunology* vol. 12 709 (2021).
11. Fu, Y., Liu, S., Zeng, S. & Shen, H. The critical roles of activated stellate cells-mediated paracrine signaling, metabolism and onco-immunology in pancreatic ductal adenocarcinoma. *Molecular Cancer* vol. 17 (2018).
12. Hidalgo, M. *et al.* Addressing the challenges of pancreatic cancer: Future directions for improving outcomes. *Pancreatology* vol. 15 8–18 (2015).
13. Bynigeri, R. R. *et al.* Pancreatic stellate cell: Pandora's box for pancreatic disease biology. *World J. Gastroenterol.* **23**, 382 (2017).
14. Hruban, R. H. *et al.* Pathology of genetically engineered mouse models of pancreatic exocrine cancer: Consensus report and recommendations. *Cancer Res.* **66**, 95–106 (2006).
15. Chari, S. T. Detecting Early Pancreatic Cancer: Problems and Prospects. *Semin. Oncol.* **34**, 284–294 (2007).
16. Cui, S. J. *et al.* Role of imaging biomarkers for prognostic prediction in patients with pancreatic ductal adenocarcinoma. *Clin. Radiol.* (2020) doi:10.1016/j.crad.2019.12.023.
17. Cave, D. D. *et al.* The revolutionary roads to study cell–cell interactions in 3d in vitro pancreatic cancer models. *Cancers (Basel).* **13**, 1–19 (2021).
18. Osuna de la Peña, D. *et al.* Bioengineered 3D models of human pancreatic cancer recapitulate in vivo tumour biology. *Nat. Commun. 2021 121* **12**, 1–15 (2021).
19. Haque, M. R. *et al.* Organ-Chip Models: Opportunities for Precision Medicine in Pancreatic Cancer. *Cancers (Basel).* **13**, 4487 (2021).
20. Mollica, H. *et al.* A 3D pancreatic tumor model to study T cell infiltration. *Biomater. Sci.* **9**, 7420–7431 (2021).
21. Schuster, B. *et al.* Automated microfluidic platform for

dynamic and combinatorial drug screening of tumor organoids. *Nat. Commun.* **11**, 1–12 (2020).
22. Nguyen, D. H. T. *et al.* A biomimetic pancreatic cancer on-chip reveals endothelial ablation via ALK7 signaling. *Sci. Adv.* **5**, 1–10 (2019).
23. Xu, H. *et al.* Organoid technology and applications in cancer research. *J. Hematol. Oncol.* **11**, 116 (2018).
24. Boj, S. F. *et al.* Organoid models of human and mouse ductal pancreatic cancer. *Cell* **160**, 324–338 (2015).
25. Beer, M. *et al.* A novel microfluidic 3D platform for culturing pancreatic ductal adenocarcinoma cells: Comparison with in vitro cultures and in vivo xenografts. *Sci. Rep.* **7**, 1–12 (2017).
26. Kramer, B. *et al.* Interstitial flow recapitulates gemcitabine chemoresistance in a 3D microfluidic pancreatic ductal adenocarcinoma model by induction of multidrug resistance proteins. *Int. J. Mol. Sci.* **20**, (2019).
27. Swayden, M., Soubeyran, P. & Iovanna, J. Upcoming Revolutionary Paths in Preclinical Modeling of Pancreatic Adenocarcinoma. *Front. Oncol.* **9**, 1443 (2020).
28. Tomás-Bort, E., Kieler, M., Sharma, S., Candido, J. B. & Loessner, D. 3D approaches to model the tumor microenvironment of pancreatic cancer. *Theranostics* vol. 10 5074–5089 (2020).
29. Low, L. A., Mummery, C., Berridge, B. R., Austin, C. P. & Tagle, D. A. Organs-on-chips: into the next decade. *Nature Reviews Drug Discovery* vol. 20 345–361 (2021).
30. Bhatia, S. N. & Ingber, D. E. Microfluidic organs-on-chips. *Nat. Biotechnol. 2014 328* **32**, 760–772 (2014).
31. Gioeli, D. *et al.* Development of a multicellular pancreatic tumor microenvironment system using patient-derived tumor cells. *Lab Chip* **19**, 1193–1204 (2019).
32. Bradney, M. J., Venis, S. M., Yang, Y., Konieczny, S. F. & Han, B. A Biomimetic Tumor Model of Heterogeneous Invasion in Pancreatic Ductal Adenocarcinoma. *Small* **1905500**, 1–10 (2020).
33. Lee, J. H. *et al.* Microfluidic co-culture of pancreatic tumor spheroids with stellate cells as a novel 3D model for investigation of stroma-mediated cell motility and drug resistance. *J. Exp. Clin. Cancer Res.* **37**, 1–12 (2018).
34. Lai, B. F. L. *et al.* Recapitulating Pancreatic Tumor Microenvironment through Synergistic Use of Patient Organoids and Organ-on-a-Chip Vasculature. *Adv. Funct. Mater.* 2000545 (2020) doi:10.1002/adfm.202000545.
35. Giuntoli, G. *et al.* In-vitro Characterization of a Hernia Mesh Featuring a Nanostructured Coating. *Front. Bioeng. Biotechnol.* **8**, (2021).
36. Licciardello, M., Ciardelli, G. & Tonda-Turo, C. Biocompatible Electrospun Polycaprolactone-Polyaniline Scaffold Treated with Atmospheric Plasma to Improve Hydrophilicity. *Bioengineering* **8**, 1–18 (2021).
37. Licciardello, M., Tonda-Turo, C., Gallina, A., Ciofani, G. & Ciardelli, G. Fabrication of extracellular matrix-like membranes for loading piezoelectric nanoparticles. *J. Phys. Mater.* **3**, 034004 (2020).
38. Tonda-Turo, C. *et al.* Crosslinked gelatin nanofibres: Preparation, characterisation and in vitro studies using glial-like cells. *Mater. Sci. Eng. C* **33**, 2723–2735 (2013).
39. Gautam, S., Dinda, A. K. & Mishra, N. C. Fabrication and characterization of PCL/gelatin composite nanofibrous scaffold for tissue engineering applications by electrospinning method. *Mater. Sci. Eng. C* **33**, 1228–1235 (2013).
40. Denis, P., Dulnik, J. & Sajkiewicz, P. Electrospinning and Structure of Bicomponent Polycaprolactone/Gelatin Nanofibers Obtained Using Alternative Solvent System. *http://dx.doi.org/10.1080/00914037.2014.945208* **64**, 354–364 (2014).
41. Binulal, N. S. *et al.* PCL–gelatin composite nanofibers electrospun using diluted acetic acid–ethyl acetate solvent system for stem cell-based bone tissue engineering. *http://dx.doi.org/10.1080/09205063.2013.859872* **25**, 325–340 (2014).
42. Gil-Castell, O., Badia, J. D., Strömberg, E., Karlsson, S. & Ribes-Greus, A. Effect of the dissolution time into an acid hydrolytic solvent to tailor electrospun nanofibrous polycaprolactone scaffolds. *Eur. Polym. J.* **87**, 174–187 (2017).
43. Mahony, O. *et al.* Hybrid Materials: Silica-Gelatin Hybrids with Tailorable Degradation and Mechanical Properties for Tissue Regeneration (Adv. Funct. Mater. 22/2010). *Adv. Funct. Mater.* **20**, 3808–3808 (2010).
44. Lee, J. H. *et al.* Microfluidic co-culture of pancreatic tumor spheroids with stellate cells as a novel 3D model for investigation of stroma-mediated cell motility and drug resistance. *J. Exp. Clin. Cancer Res.* **37**, 1–12 (2018).
45. Jeong, S. Y., Lee, J. H., Shin, Y., Chung, S. & Kuh, H. J. Co-culture of tumor spheroids and fibroblasts in a collagen matrix-incorporated microfluidic chip mimics reciprocal activation in solid tumor microenvironment. *PLoS One* **11**, e0159013 (2016).
46. Fujiwara, M., Kanayama, K., Hirokawa, Y. S. & Shiraishi, T. ASF-4-1 fibroblast-rich culture increases chemoresistance and mTOR expression of pancreatic cancer BxPC-3 cells at the invasive front in vitro, and promotes tumor growth and invasion in vivo. *Oncol. Lett.* **11**, 2773 (2016).
47. Wang, P. & Zhu, Z. Prognostic and Clinicopathological Significance of E-Cadherin in Pancreatic Cancer Patients: A Meta-Analysis. *Front. Oncol.* **11**, 938 (2021).
48. Golan, T. *et al.* Ascites-derived pancreatic ductal adenocarcinoma primary cell cultures as a platform for personalised medicine. *Br. J. Cancer 2014 1109* **110**, 2269–2276 (2014).
49. Liang, C. *et al.* Complex roles of the stroma in the intrinsic resistance to gemcitabine in pancreatic cancer: where we are and where we are going. *Exp. Mol. Med. 2017 4912* **49**, e406–e406 (2017).
50. Procacci, P., Moscheni, C., Sartori, P., Sommariva, M. & Gagliano, N. Tumor–Stroma Cross-Talk in Human Pancreatic Ductal Adenocarcinoma: A Focus on the Effect of the Extracellular Matrix on Tumor Cell Phenotype and Invasive Potential. *Cells 2018, Vol. 7, Page 158* **7**, 158 (2018).
51. Matsuzawa, A. *et al.* Pancreatic Cancer and Cellular Senescence: Tumor Microenvironment under the Spotlight. *Int. J. Mol. Sci. 2022, Vol. 23, Page 254* **23**, 254 (2021).

52. Thomas, D. & Radhakrishnan, P. Tumor-stromal crosstalk in pancreatic cancer and tissue fibrosis. *Mol. Cancer* **18**, (2019).
53. Hadden, M. *et al.* Mechanically stressed cancer microenvironment: Role in pancreatic cancer progression. *Biochim. Biophys. Acta - Rev. Cancer* **1874**, 188418 (2020).
54. Gardian, K., Janczewska, S., Olszewski, W. L. & Durlik, M. Analysis of Pancreatic Cancer Microenvironment: Role of Macrophage Infiltrates and Growth Factors Expression. *J. Cancer* **3**, 285 (2012).
55. Farrow, B., Albo, D. & Berger, D. H. The Role of the Tumor Microenvironment in the Progression of Pancreatic Cancer. *J. Surg. Res.* **149**, 319–328 (2008).
56. Ho, W. J., Jaffee, E. M. & Zheng, L. The tumour microenvironment in pancreatic cancer — clinical challenges and opportunities. *Nature Reviews Clinical Oncology* vol. 17 527–540 (2020).
57. Sperb, N., Tsesmelis, M. & Wirth, T. Crosstalk between tumor and stromal cells in pancreatic ductal adenocarcinoma. *International Journal of Molecular Sciences* vol. 21 1–23 (2020).
58. Lazzari, G. *et al.* Multicellular spheroid based on a triple co-culture: A novel 3D model to mimic pancreatic tumor complexity. *Acta Biomater.* **78**, 296–307 (2018).
59. Brancato, V. *et al.* Bioengineered tumoral microtissues recapitulate desmoplastic reaction of pancreatic cancer. *Acta Biomater.* **49**, 152–166 (2017).
60. Gupta, P. *et al.* A Novel Scaffold-Based Hybrid Multicellular Model for Pancreatic Ductal Adenocarcinoma—Toward a Better Mimicry of the in vivo Tumor Microenvironment. *Front. Bioeng. Biotechnol.* **8**, (2020).
61. Norberg, K. J. *et al.* A novel pancreatic tumour and stellate cell 3D co-culture spheroid model. *BMC Cancer* **20**, 475 (2020).
62. Yu, Y. *et al.* Preclinical models of pancreatic ductal adenocarcinoma: challenges and opportunities in the era of precision medicine. *Journal of Experimental and Clinical Cancer Research* vol. 40 1–13 (2021).
63. Gündel, B., Liu, X., Löhr, M. & Heuchel, R. Pancreatic Ductal Adenocarcinoma: Preclinical in vitro and ex vivo Models. *Front. Cell Dev. Biol.* **9**, 1–12 (2021).
64. Uzunparmak, B. & Sahin, I. H. Pancreatic cancer microenvironment: a current dilemma. *Clin. Transl. Med. 2019 81* **8**, 1–8 (2019).
65. Li, K., Liu, T., Chen, J., Ni, H. & Li, W. Survivin in breast cancer-derived exosomes activates fibroblasts by up-regulating SOD1, whose feedback promotes cancer proliferation and metastasis. *J. Biol. Chem.* **295**, 13737–13752 (2020).
66. Guo, X., Oshima, H., Kitmura, T., Taketo, M. M. & Oshima, M. Stromal fibroblasts activated by tumor cells promote angiogenesis in mouse gastric cancer. *J. Biol. Chem.* **283**, 19864–19871 (2008).
67. Cheng, C. *et al.* Construction and Analysis of an Integrated Regulatory Network Derived from High-Throughput Sequencing Data. *PLOS Comput. Biol.* **7**, e1002190 (2011).
68. Cai, J. *et al.* Fibroblasts in omentum activated by tumor cells promote ovarian cancer growth, adhesion and invasiveness. *Carcinogenesis* **33**, 20–29 (2012).
69. Omary, M. B., Lugea, A., Lowe, A. W. & Pandol, S. J. The pancreatic stellate cell: A star on the rise in pancreatic diseases. *Journal of Clinical Investigation* vol. 117 50–59 (2007).
70. Buchholz Hans Kestler Karlheinz Holzmann Volker Ellenrieder Wilhelm Schneiderhan Marco Siech Guido Adler Max G Bachem Thomas M Gress, M. A. Transcriptome analysis of human hepatic and pancreatic stellate cells: organ-specific variations of a common transcriptional phenotype. *J Mol Med* **83**, 795–805 (2005).
71. Ohuchida, K. *et al.* Radiation to Stromal Fibroblasts Increases Invasiveness of Pancreatic Cancer Cells through Tumor-Stromal Interactions. *Cancer Res.* **64**, 3215–3222 (2004).
72. Damhofer, H. *et al.* Assessment of the stromal contribution to Sonic Hedgehog-dependent pancreatic adenocarcinoma mRNA-Seq. (2013) doi:10.1016/j.molonc.2013.08.004.
73. Majety, M., Pradel, L. P., Gies, M. & Ries, C. H. Fibroblasts Influence Survival and Therapeutic Response in a 3D Co-Culture Model. (2015) doi:10.1371/journal.pone.0127948.
74. Monteiro, M. V, Ferreira, L. P., Rocha, M., Gaspar, V. M. & Mano, J. F. Journal Pre-proof Advances in bioengineering pancreatic tumor-stroma physiomimetic Biomodels. *Biomaterials* (2022) doi:10.1016/j.biomaterials.2022.121653.
75. Ji, Z., Mei, F. C., Xie, J. & Cheng, X. Oncogenic KRAS activates hedgehog signaling pathway in pancreatic cancer cells. *J. Biol. Chem.* **282**, 14048–14055 (2007).
76. Brentnall, T. A. *et al.* Arousal of Cancer-Associated Stroma: Overexpression of Palladin Activates Fibroblasts to Promote Tumor Invasion. *PLoS One* **7**, (2012).
77. Zhou, H. *et al.* SOX9 activity is induced by oncogenic Kras to affect MDC1 and MCMs expression in pancreatic cancer. *Oncogene 2018 377* **37**, 912–923 (2017).
78. Pandiri, A. R. Overview of exocrine pancreatic pathobiology. *Toxicol. Pathol.* **42**, 207–216 (2014).
79. Shields, M. A., Dangi-Garimella, S., Krantz, S. B., Bentrem, D. J. & Munshi, H. G. Pancreatic Cancer Cells Respond to Type I Collagen by Inducing Snail Expression to Promote Membrane Type 1 Matrix Metalloproteinase-dependent Collagen Invasion. *J. Biol. Chem.* **286**, 10495 (2011).
80. Bott, K. *et al.* The effect of matrix characteristics on fibroblast proliferation in 3D gels. *Biomaterials* **31**, 8454–8464 (2010).
81. Tabatabaei, F., Moharamzadeh, K. & Tayebi, L. Fibroblast encapsulation in gelatin methacryloyl (GelMA) versus collagen hydrogel as substrates for oral mucosa tissue engineering. *J. Oral Biol. Craniofacial Res.* **10**, 573–577 (2020).
82. Baena, J. M. *et al.* Volume-by-volume bioprinting of chondrocytes-alginate bioinks in high temperature thermoplastic scaffolds for cartilage regeneration. *Exp. Biol. Med.* **244**, 13–21 (2019).
83. Hwang, H. J., Oh, M. S., Lee, D. W. & Kuh, H. J. Multiplex quantitative analysis of stroma-mediated cancer cell invasion, matrix remodeling, and drug response in a 3D co-culture model of pancreatic tumor spheroids and stellate

cells. *J. Exp. Clin. Cancer Res.* **38**, (2019).
84. Li, J., Chen, B., Fellows, G. F., Goodyer, C. G. & Wang, R. Activation of Pancreatic Stellate Cells Is Beneficial for Exocrine but Not Endocrine Cell Differentiation in the Developing Human Pancreas. *Front. Cell Dev. Biol.* **9**, 1769 (2021).
85. Paoli, C. & Carrer, A. Organotypic Culture of Acinar Cells for the Study of Pancreatic Cancer Initiation. *Cancers (Basel).* **12**, 1–22 (2020).
86. Cantara, S. I. *et al.* Selective functionalization of nanofiber scaffolds to regulate salivary gland epithelial cell proliferation and polarity. *Biomaterials* **33**, 8372–8382 (2012).
87. Buscemi, S. *et al.* Electrospun Polyhydroxyethyl-Aspartamide–Polylactic Acid Scaffold for Biliary Duct Repair: A Preliminary In Vivo Evaluation. *Transplant. Proc.* **49**, 711–715 (2017).
88. Nelson, M. T. *et al.* Preferential, enhanced breast cancer cell migration on biomimetic electrospun nanofiber 'cell highways'. *BMC Cancer* **14**, 1–16 (2014).
89. Leong, M. F., Chian, K. S., Mhaisalkar, P. S., Ong, W. F. & Ratner, B. D. Effect of electrospun poly(D,L-lactide) fibrous scaffold with nanoporous surface on attachment of porcine esophageal epithelial cells and protein adsorption. *J. Biomed. Mater. Res. Part A* **89A**, 1040–1048 (2009).
90. Burton, T. P., Corcoran, A. & Callanan, A. The effect of electrospun polycaprolactone scaffold morphology on human kidney epithelial cells. *Biomed. Mater.* **13**, 015006 (2017).
91. Mendle, J. H. *et al.* Bortezomib and gemcitabine in relapsed or refractory Hodgkin's lymphoma. *Ann. Oncol.* **19**, 1759 (2008).